Numerical Simulation of Broken Ice Cover Forces on Structures: a Parametric Study

Sayed, Mohamed; Frederking, Robert; Barker, Anne

Publisher's version / Version de l'éditeur:

Proceedings of 10th International Offshore and Polar Engineering Conference (ISOPE), 1, pp. 656-662, 2000

Proceedings of the Tenth (2000) International Offshore and Polar Engineering Conference
ISOPE'00, Vol. 1, pp 656-662. Seattle, USA. 2000

Numerical Simulation of Broken Ice Cover Forces on Structures: a Parametric Study

Mohamed Sayed, Robert Frederking, and Anne Barker
Canadian Hydraulics Centre, National Research Council
Ottawa, Ontario, Canada K1A 0R6
Mohamed.Sayed@nrc.ca Robert.Frederking@nrc.ca Anne.Barker@nrc.ca

ABSTRACT
A numerical model of broken ice cover interaction with offshore structures is presented. The model is based on using a Particle-In-Cell (PIC) approach to advect the ice cover, and a Mohr-Coulomb plastic yield criterion to describe ice properties. The Zhang-Hibler (1997) numerical scheme is used to solve the momentum equations. A parametric study was conducted in order to determine the influence of shape of the structure, ice thickness, ice properties, and velocity on the resulting ice forces.

1. INTRODUCTION

Ice forces on structures in drifting broken ice are a concern for offshore petroleum production operations off the East Coast of Canada. Methods for estimating those forces, however, remain uncertain. Empirical formulas (e.g. Korzhavin, 1971) have so far been extensively used for design purposes. The pervasiveness of such formulas is the result of their excessive simplicity and the lack of more rigorous methods. However, the simplicity of empirical formulas encompasses gross inaccuracies, which usually produce high estimates of ice forces. For example, the empirical formulas cannot account for specific geometries of structure and ice features, inertial effects, details of ice properties, interaction modes, and forcing conditions.

The complexity of ice-structure interaction also poses several difficulties to numerical modelling. Many interaction scenarios include discontinuities (e.g. in stress and velocity fields), moving and free boundaries, propagation of large cracks, and large deformations. Other less severe difficulties include complex ice rheology and transient behaviour. Consequently, most traditional approaches of numerical modelling had limited success when used to examine ice-structure interaction.

A number of approaches for numerical modelling of ice-structure interaction have been pursued. We only refer to a few recent relevant publications here, which include several references to the available literature. One class of models is based on finite element solutions and continuum constitutive equations. For example, Sand and Horrigmoe (1998) developed a plasticity solution for forces on sloping structures. Another study by Choi and Hwang (1998) used a continuum damage criterion to estimate indentation forces. In order to deal with discontinuities and large cracks, discrete element approaches were used. These approaches include work by Sayed (1997), Katsuragi et al. (1998), and Sayed and Timco (1999). The results of those studies show that considerable details of deformation processes can be obtained, albeit at substantial computational cost.

The present study concerns a class of problems where the behaviour of the ice cover can be modeled using a continuum cohesionless Mohr-Coulomb criterion. Broken ice fields belong to such a class. Since such ice covers consist of broken floes with no apparent frozen bonds between them, it may be intuitively expected that the tensile strength would be negligible. Consequently, as may be seen from the well-known graphical representation of the Mohr-Coulomb criterion, the shear strength (and cohesion) would be negligible. We can only rely on this plausible intuitive view, in the absence of any relevant field measurements. The continuum formulation also excludes cases where a single (or a few) relatively large floes impact the structure.

The model is based on a Particle-In-Cell (PIC) approach, combined with a viscous plastic ice rheology. The PIC model is semi-Lagrangian. It uses discrete particles to model ice advection, while solving the momentum equations over an Eulerian grid. The use of discrete particles reduces numerical diffusion, and improves the accuracy of modelling ice boundary conditions. At the same time, the use of an Eulerian grid makes it possible to utilize an implicit numerical solution scheme for the momentum equations, which substantially increases the computational efficiency.

Several of the ideas used in the present model were originally developed for ice forecasting, at larger scales than ice-structure interaction problems. The viscous plastic formulation that numerically approximates the rigid-plastic behaviour was first developed by Hibler (1979). Flato (1993) implemented a PIC model in an ice forecasting program, and showed that it improves the accuracy. Finally, the present implicit numerical solution of the momentum equations follows an efficient scheme devised by Zhang and Hibler (1997). The present model is adapted from an operational ice forecasting model developed by Sayed and Carrieres (1999). A notable difference, though, is the use of the Mohr-Coulomb yield criterion in the present model instead of the elliptical yield envelope of Hibler (1979).

2. MODEL

2.1 Overview

For the Particle-In-Cell (PIC) approach, the ice cover is conceptually represented by discrete particles that are individually advected. The

term *advection* is used here to refer to integrating a particle's velocity with respect to time, and thus determining the new position (or coordinates). Therefore, the approach can be viewed as a hybrid method. Particles are used to model advection and keep track of ice thickness and concentration (or area coverage). The momentum equations, however, are solved over a fixed (or Eulerian) grid. Continuum equations are also used to describe the rheology of the ice.

In the two-dimensional PIC formulation, each particle is considered to have an area and a volume. The area of a particle can decrease if the pressure exceeds a certain limit (i.e. ridging pressure). The volume, however, remains constant. Thus, if a particle is subjected to relatively high pressures, its area may decrease, and its thickness would correspondingly increase (constant volume = area x thickness). Note that the particles are not actual ice floes, but computational constructs.

At each time step, the areas of the particles are *mapped* to a fixed grid; i.e. the areas of the particles are converted to continuum ice concentration values (area of ice/ total area) for each cell of the grid. Similarly, the thicknesses of the particles are converted to continuum ice thickness values at the cells of the grid. Such mapping from the particles to the fixed grid is done using a *weighting function*. Thus, when calculating ice concentration for a cell in the fixed grid, particles closer to the cell centre are given higher weight than those farther away.

Once values of ice concentration and thickness are over the fixed grid, the continuum momentum and rheology equations are solved over that grid. Those continuum equations can thus be solved in an efficient way. The use of a fixed grid makes it possible to employ *implicit* numerical methods, which are efficient. The time steps can be very large compared to explicit formulations that must be used, for example, in discrete element methods. In the present model, the numerical method of Zhang and Hibler (1997) is used because of its efficiency.

The solution of the momentum and rheology equations gives velocity values at the nodes of the fixed grid. Those velocities are mapped from the nodes to the particles in a manner similar to that discussed above. The particles are then advected to new positions.

2.2 Governing Equations

The governing equations consist of:

- Continuum linear momentum equations.
- Continuum rheology, which is represented here by a viscous plastic model of Mohr-Coulomb yield criterion.
- Mapping functions to convert particles' areas and thicknesses to continuum values on the fixed grid, and to convert velocities at the grid nodes to velocities for each particle.

The momentum equations are expressed as

$$mass_{ice}\frac{d\vec{u}}{dt} = \nabla\cdot\sigma + \vec{\tau}_a + \vec{\tau}_w \tag{2.1}$$

where $mass_{ice}$ is the mass of the ice cover per unit area ($mass_{ice} = \rho_{ice}\, h$), ρ_{ice} is ice density, h is the ice thickness, $\vec{u}$ is the velocity vector, σ is the stress tensor, and $\vec{\tau}_a$ and $\vec{\tau}_w$ are the air and water drag stresses. The air and water drag stresses are given by the following quadratic formulas

$$\vec{\tau}_a = c_a \rho_a \left|\vec{\mathbf{U}}_a\right| \vec{\mathbf{U}}_a \tag{2.2}$$

and

$$\vec{\tau}_w = c_w \rho_w \left|\vec{\mathbf{U}}_w - \vec{u}\right| \left(\vec{\mathbf{U}}_w - \vec{u}\right) \tag{2.3}$$

where c_a and c_w are the air and water drag coefficients, $\vec{U}_a$ is wind velocity, $\vec{U}_w$ is water velocity, and ρ_a and ρ_w are the air and water densities, respectively. Eq.(2.2) assumes that ice velocity is small compared to wind velocity.

The stress-strain rate relationship is given by

$$\sigma_{ij} = -p\delta_{ij} + 2\eta\,\dot{\varepsilon}_{ij} + (\zeta - \eta)\dot{\varepsilon}_{kk}\,\delta_{ij} \tag{2.4}$$

where $\dot{\varepsilon}_{ij}$ is the strain rate, p is the mean normal stress, η is the shear viscosity, and ζ is the bulk viscosity. Note that $\dot{\varepsilon}_{kk}$ is the volumetric strain rate. The bulk viscosity, ζ, is difficult to measure or infer because relatively large rates of change of density must be used. It is common, however, to assume that either (ζ-η) or ζ is negligible. We assume here that the bulk viscosity, ζ, is zero. An advantage of this assumption is that the resulting ratio between the principal stresses agrees with the Mohr-Coulomb criterion, which will be discussed below.

The mean normal stress, p, is usually considered to increase with increasing ice concentration, A (area of ice/total area). We use a formula analogous to that of Hibler (1979). Note, however, that p is defined according to the common convention in continuum mechanics literature, and is different from the strength P used by Hibler (1979) by a factor of two.

$$p = P^* h_{ice} \exp\left(-K(1-A)\right) \tag{2.5}$$

where P^* is a reference ice strength, and K is a constant.

The Mohr-Coulomb criterion is introduced by giving the shear viscosity, η, the following value

$$\eta = \frac{p\sin\phi}{\Delta} \tag{2.6}$$

where ϕ is the angle of internal friction. The strain rate Δ is given by

$$\Delta = \max\left(\left|\dot{\varepsilon}_1 - \dot{\varepsilon}_2\right|, \dot{\varepsilon}_0\right) \tag{2.7}$$

where $\dot{\varepsilon}_1$ and $\dot{\varepsilon}_2$ are the principal strain rates and $\dot{\varepsilon}_0$ is a threshold strain rate. For relatively large strain rates, $\Delta > \dot{\varepsilon}_0$, the rheology is plastic and the yield criterion is satisfied. At small rates of deformation, however, the shear viscosity becomes constant, and the corresponding rheology would be viscous. A very small threshold strain rate (typically $\dot{\varepsilon}_0 = 10^{-20}\ s^{-1}$) is used in order to maintain a predominantly plastic deformation. It can be seen by substituting Eq. (2.6) in Eq. (2.4), that the ratio between the principal stresses is $\left(\frac{1+\sin\phi}{1-\sin\phi}\right)$, which is a well-known characteristic of Mohr-Coulomb criterion.

The above value of $\dot{\varepsilon}_0$ was chosen by testing a range of values. Using smaller values did not produce any noticeable differences in the results. This indicates that deformation was predominantly plastic. The above value is also commensurate with that used by Hibler (1979), albeit for larger geophysical length scale. Nonetheless, the present value of $\dot{\varepsilon}_0$, should not be extrapolated to other problems without ensuring that it is sufficiently small. A tension cut-off value is further introduced in the model. If a tensile stress develops, the viscosity coefficient, η, is adjusted such that the maximum principal stress is set equal to zero.

The preceding set of equations, together with PIC advection, is sufficient to determine the stresses, velocities, and configuration of the ice cover through its interaction with a structure. The PIC scheme and the interpolation functions used to map variables between the particles and fixed grid are discussed in Appendix A.

2.3 Numerical Approach

The solution is implemented using a staggered grid. The velocity components are defined at the corners of the velocity grid. All scalar values (pressure, viscosities, thickness and concentration) are defined at the centres of the grid cells.

Starting from a given initial configuration, the numerical solution of the above governing equations updates the velocities, pressures, thicknesses, and concentrations at each time step. The main logic of the solution consists of the following steps:

- Advect the particles to new positions (Appendix A).
- Determine the thickness and concentration values by interpolating the area and volume of the particles to the scalar grid (Appendix A).
- Correct the thickness and concentration values by adjusting concentrations higher than unity. Next, correct the area and thickness of each particle (Appendix A).
- Calculate the pressures on the scalar grid using Eq.(2.5).
- Solve the momentum equations Eq.(2.1). The numerical approach is briefly discussed in Appendix B.
- Determine particle velocities by interpolating values from the velocity grid (Appendix A).

A *no-slip* boundary condition was used to define the structure. This condition was implemented via a mask, setting velocities to zero for all nodes within the structure. Another *full-slip* condition was used at the top and bottom boundaries of the grid. Particles were prevented from moving through those boundaries but allowed to move parallel to them in order to satisfy that condition. For example, if a particle moved upwards through the top boundary, its y-position is reset to a value immediately below the boundary, without changing its x-position.

The PIC approach does not require imposing conditions at the free interface between the ice cover and open water (e.g. leads). At such interfaces, the particles can move according to the governing equations, and the free interface evolves. It is important, however, to use the appropriate velocity values at open water nodes since they influence both the solution of the momentum equations and velocity interpolation from the grid to the particles. The approach used in the present study was to solve the momentum equations over all open water nodes. That procedure requires introducing a minimum value of ice thickness at such nodes to avoid numerical problems.

3. TEST CASES

Four shapes of the structure were examined: circular, square, diamond and octagonal. The width of all structures perpendicular to the ice movement direction was the same (100m). A fifth structure, the square rotated 45°, was also tested. Its width, normal to the ice movement direction, was 141 m. These structures were selected to represent a range of generic structure shapes which offshore production structures might take. There is a wide range of such structures and they are best dealt with on a case by case basis.

The ice cover parameters that were varied in the study included thickness, velocity, and the angle of internal friction, ϕ. The threshold strain rate, $\dot{\varepsilon}_0$ was chosen small enough so as to have no effect on the results. In the formulation of the problem, it is assumed that the ice cover behaves as a continuum, thus floe size does not appear explicitly in the formulation. There are no measurements to specify the maximum floe size, beyond which the continuum idealization breaks-down. A rule of thumb, often mentioned in literature on the behaviour of granular materials (e.g. Brown and Richards, 1970) is that the maximum particle size should be smaller than about 20% of the relevant length scale (in this case, the structure's width). Floe size is a factor that has been observed to effect ice forces, so this is a factor that eventually has to be taken into account. In the present formulation, the angle of internal friction, ϕ, account for the overall ice cover properties, including the effects of floe size, and interlocking and friction between floes. The other factor that characterizes the ice cover is concentration. For this study, an initial value of 0.8 was assumed at the start of each simulation run.

The results of a *base* case will be presented in detail to demonstrate the insights the simulation can deliver. A schematic of the structure, in this case circular, and the calculation grid is presented in Fig. 1. The grid is 50 nodes wide and 130 nodes long. Each grid cell is 10 m, thus 11 grid points define the structure width of 100 m. The base case was for 1 m thick ice, with an internal friction angle of 40°, and a velocity of 0.5 m/s. Preliminary runs showed that a P^* of 15 kPa appears to give reasonable results (with no detectable ridging as observed in field conditions mentioned below). While decreasing the value of P^* increases ridging, increasing it did not affect predicted stresses. The ice cover initially extends from node #30 to node #130. The area from node #0 to node #30 was left empty to provide space for the ice cover to move to the left, unhindered in the x-direction. Tests were done using different grid sizes. Those tests showed that the chosen value of grid cell size has no effect on the results.

Approximately 30 particles were used for each grid cell (corresponding to a concentration of 1). Lower concentration values of a cell were represented by proportionally fewer particles. Particles were initially placed at approximately equal intervals for each grid cell. Their positions cannot be plotted (e.g. in Fig. 1) because of their large number. We also note that in some cases the initial placement of the particles was not perfectly symmetrical about the x-axis. Consequently, some of the results below (e.g. stress distributions) show slight asymmetry.

Figure 2 shows the force on the structure in the x-direction (direction of ice motion), for base case conditions. This force was calculated by taking the average of the stresses in the x-direction on a 100 m long line along the x-axis node #51 from y-axis node #20 to #30. The force reaches a maximum value after approximately 120 s from the start of the run, and slightly drops afterwards. The force component acting on the structure in the y-direction is negligible.

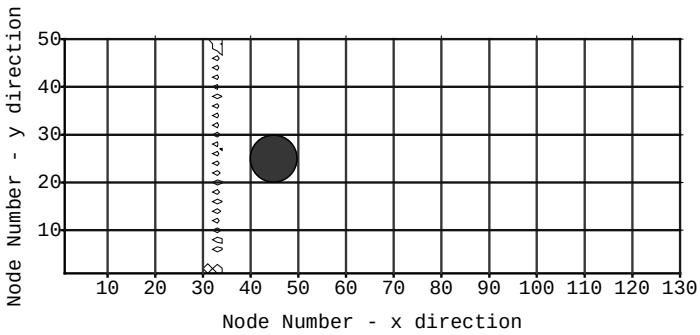

Figure 1 Schematic of structure and numerical grid

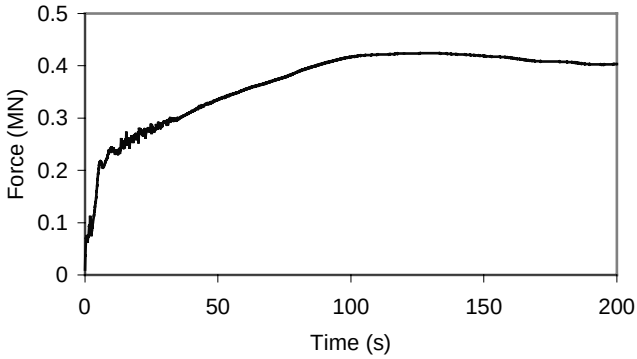

Figure 2 Total ice force in x-direction on 100 diameter structure, h=1m, V=0.5 m/s and ϕ=40°

The results determine the evolution of the stress, velocity, concentration, and thickness. As an example, further results from the base case are presented. Figure 3 shows the concentration 120 s into the simulation. This snapshot corresponds to the maximum force on the structure. Figure 3 shows a high concentration area developing in front of the structure. Also, a wake develops downstream from the structure. These are qualitative observations that agree with field observations, and hence lend confidence to the simulation. Figure 4 shows the distribution of the normal stress in the x-direction at time = 120 s, with compressive stress shown positive. The maximum stress at the structure is approximately 10 kPa. The development and expansion of an area of high stress in front of the structure is apparent. Figure 5 shows plots of the velocity vectors at 120 s. The figure shows a zone of slowing velocity, extending about two and a half structure diameters upstream, and a wake downstream from the structure.

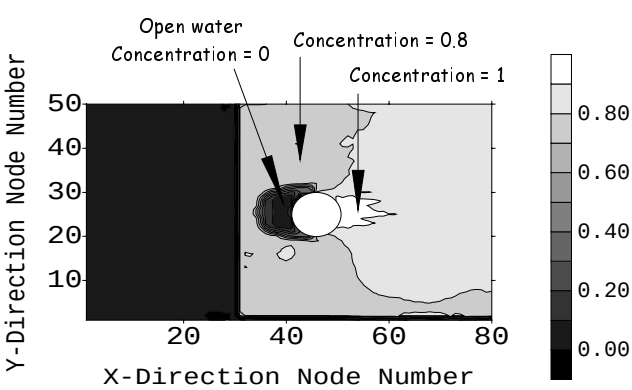

Figure 3 Ice concentration 120 s into the simulation of Run_1, h=1m, V=0.5 m/s and ϕ=40°

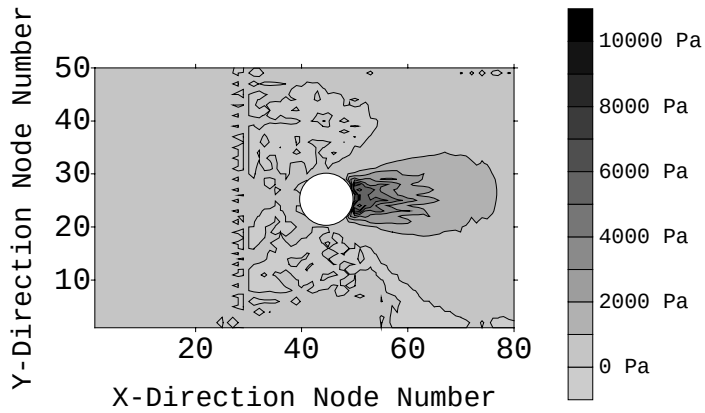

Figure 4 Normal stress in x-direction 120 s into the simulation of Run_1, h=1m, V=0.5 m/s and ϕ=40°

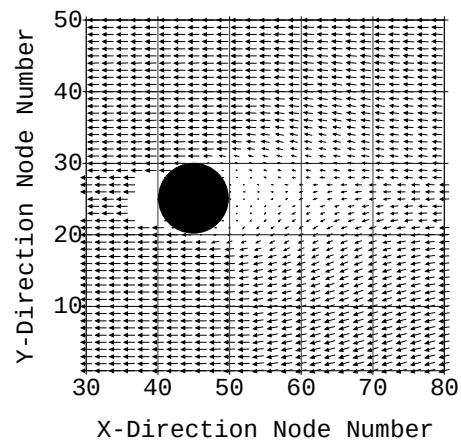

Figure 5 Velocity field 120 s into the simulation of Run_1, h=1m, V=0.5 m/s and ϕ=40°

4. PARAMETRIC STUDY

An extensive set of runs was done in order to determine the role of geometry of the structure, ice cover properties and ice velocity. Five different structures were examined. The following ice cover properties and conditions were used:

- Ice thickness, h = 0.5, 1, 2 and 4 m
- Angle of internal friction, ϕ = 35, 40 and 45°
- Ice cover velocity, V = 0.1, 0.2 0.5 and 1 m/s

The results for the five different structures are compared in Fig. 6. For structures with a 100m wide face perpendicular to the direction of ice motion, progressively larger maximum forces were predicted for a diamond, circular, octagonal and square shape. The maximum force values are summarized in Table 1. The change of ice force with structure shape generally follows the trend observed elsewhere in the literature (e.g. Korzhavin, 1962). One surprising result is the comparison of the force on the square and the rotated square. Note that there is a slight decrease in force from the square to the rotated square, even though the width of the structure presented to the ice movement direction has increased from 100m to 141m.

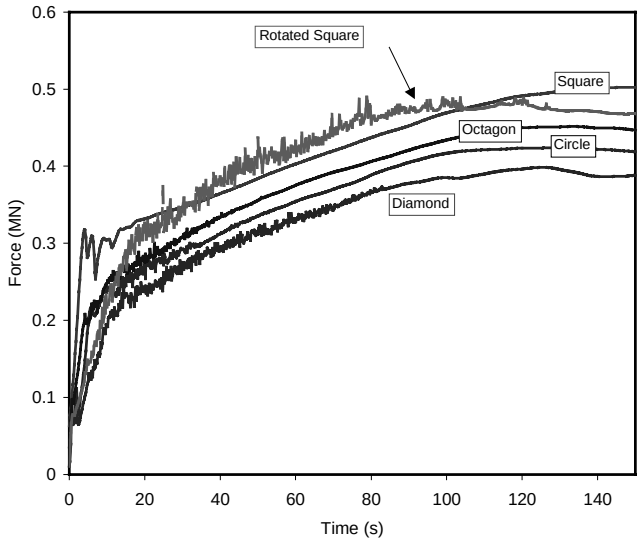

Figure 6 Total force for structures of various shapes, h=1m, V=0.5 m/s and ϕ=40°

Table 1 Maximum force values for base case conditions.

Structure	Maximum Force (MN)	Normalized Force
Square, 100 m wide	0.502	1.00
Octagon, 100 m wide	0.452	0.90
Circle, 100 m wide	0.424	0.84
Diamond, 100 m wide	0.399	0.79
Rotated Square, 141 m wide	0.490	0.98

The effects of ice thickness, internal friction angle and velocity were next examined. The effect of ice thickness on the maximum force on a circular structure is plotted in Fig. 7. Note that similar trends were seen for the other structure shapes. The influence of the angle of internal friction, ϕ, and velocity, V, are illustrated in Figs. 8 and 9.

The dependence of the total force on the structure, F_c, on each parameter is given by the following curve-fit equations. The role of ice thickness, h, is represented by

$$F_C \propto h^{1.67} \tag{4.1}$$

where ice cover thickness, h, is in meters. The effect of the internal friction effect, ϕ, is given by

$$F_C \propto \left[\frac{\sin\phi}{\sin\left(40^0\right)}\right]^{1.8} \tag{4.2}$$

Finally, the expression for velocity, V, dependence is given by

$$F_C = 0.25\exp\left(1.07V\right) \tag{4.3}$$

where V is velocity in m/s, for the base case of h = 1 m and ϕ = 40°. It is convenient to group the above three expressions as follows

$$F_C = S\left[\exp\left(1.07V\right)\right]\left[h\right]^{1.67}\left[\frac{\sin\phi}{\sin\left(40^0\right)}\right]^{1.8} \tag{4.4}$$

where S is a coefficient which accounts for the shape of the structure (i.e. S is assigned values to fit the results obtained for each shape).

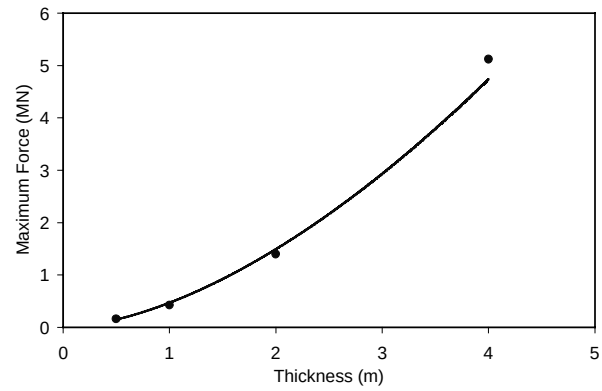

Figure 7 Total force versus ice thickness for circular structure

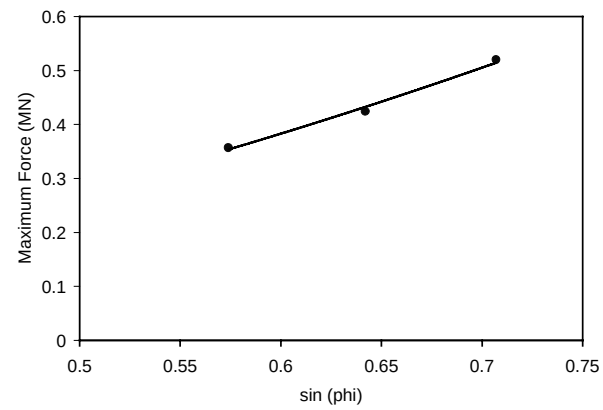

Figure 8 Total force versus sin(ϕ) for circular structure

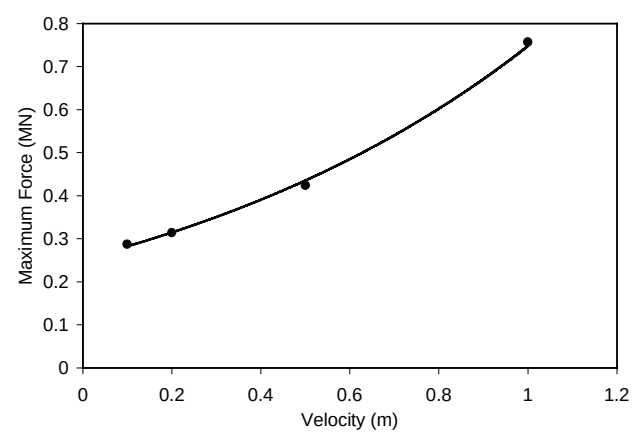

Figure 9 Total force versus ice velocity for circular structure

The multiplicative grouping of terms in Eq. (4.4) fits the results. It is, however, arbitrary and simply used here for convenience. Note that this is a dimensional equation and care must be taken to ensure correct units are applied for each input parameter. In addition, caution must be exercised in extrapolating beyond the ranges for which the original

parametric study was conducted. Equation (4.4) does not take into account structure width since all calculations were for a 100 m width of structure, except for the rotated square. The shape coefficient, S, is given in Table 2.

Table 2 Shape coefficient, S to be applied in Equation (4.4)

Structure Shape	Shape Coefficient, S
Square, 100 m wide	0.30
Octagon, 100 m wide	0.27
Circle, 100 m wide	0.25
Diamond, 100 m wide	0.24
Rotated Square, 141 m wide	0.29

Full-scale data for broken ice covers are sparse. Measurements of ice forces on the Gulf Kulluk (Wright, 1999), however, can be used to verify the magnitude of total forces. They also give some descriptive information concerning ice conditions. The Kulluk is a circular drilling unit of 70 m in diameter at the waterline. Its mooring lines were instrumented so forces on the unit due to drifting broken ice could be determined. Observations of ice conditions were also documented. Wright (1999) abstracted ice force data for various ice conditions. What he describes as "managed ice with good clearance" seems to coincide most closely with the ice properties used for the numerical simulations. This ice condition was for ice floes less than 50 m in diameter, which flowed in a "slurry"-like fashion around the Kulluk. Some of his observations were that (i) force increased linearly with ice thickness, (ii) no clear velocity effects were discernable up to speeds of 0.5 m/s, and (iii) force increased with concentration. Quantitatively the following data were extracted for validation:

- ice conditions: thickness of 2 m, floe size less than 50 m, and drift speed from .25 to 0.50 m/s.
- ice forces: less than 0.8 to 1.0 MN

Using Eq. (4.4), an ice thickness of 2 m, an internal friction angle of 30° and a velocity range of 0.25 – 0.50 m/s, the predicted force ranges from 0.66 MN to 0.86 MN. Further validation will be done in a future study, however, it can be seen that the numerical simulation force predictions agree well with full-scale data. Note that the present work concerns broken ice covers. Predicted stresses are less than those due to intact ice covers (Sanderson, 1988), as expected.

5. CONCLUSION

This paper has described a new numerical model of ice-structure interaction. The model is based on a PIC scheme for ice advection, and a viscous plastic rheology to approximate a rigid-plastic Mohr-Coulomb yield criterion. The numerical solution of the momentum equations follows the approach of Zhang-Hibler. That method leads to substantial improvements in the computational efficiency. Consequently, relatively large problems of practical significance can be examined.

The model was used to conduct a parametric study of broken ice forces on structures of various shapes. The resulting distributions of stresses, ice concentrations, and velocity appear to agree with intuitively expected trends and the available *sparse* field observations. The roles of ice thickness, ice properties, and velocity were also determined. The results were summarized in the form of empirical equations in order to make them convenient for use by interested readers.

The results of the parametric study show that ice thickness has the most significant influence on the total force, followed by ice cover properties, which are expressed in terms of an angle of internal friction. The shape of the structure appears to have a minor effect on the resulting force. We caution, however, that the preceding conclusions should be valid only for the examined range of conditions of ice cover and structure types.

6. ACKNOWLEDGEMENTS

The financial support of the Program on Energy Research and Development (PERD) is gratefully acknowledged.

7. REFERENCES

Brown, RL, Richards,JC (1970)."Principles of powder technology," Pergamon, Oxford.

Choi, K, and Hwang, OJ (1998). "Continuum damage modelling for the estimation of ice load under indentation," Proceedings ISOPE '98, Montreal, Canada, Vol. II, pp.468-475.

Flato, GM (1993). "A Particle-In-Cell sea-ice model," Atmosphere-Ocean, Vol. 31, No. 3, pp. 339-358.

Hibler, WDIII (1979). "A dynamic thermodynamic sea ice model," J. Physical Oceanography, Vol. 9, No. 4, pp. 815-846.

Katsuragi, K, Kawasaki, T, Seto, H, and Hayashi, Y. (1998)."Distinct element simulation of ice-structure interaction," Proceedings of the 8th International Offshore and Polar Engineering Conference (ISOPE '98), Montreal, Canada, Vol. II, pp.395-401.

Korzhavin, KN (1971). "Action of ice on engineering structures," US Army CRREL Translation TL260, Hanover, NH, USA.

Sand, B, and Horrigmoe, G (1998)."Simulation of ice forces on sloping structures," Proceedings ISOPE '98, Montreal, Canada, Vol. II, pp.476-482.

Sanderson, TJO (1988)."Ice Mechanics: Risks to Offshore Structures," Graham and Trotman.

Sayed. M, 1997. Discrete and Lattice Models of Floating Ice Covers, Proceedings of the 7th International Offshore and Polar Engineering Conference (ISOPE '97), Honolulu, Vol. II, pp.428-433.

Sayed, M (1998)."Ice model development: implementation," Technical Report HYD-TR-036, Canadian Hydraulics Centre, National Research Council, Ottawa, Ontario, Canada, June 1998.

Sayed, M, and Carrieres, T (1999)."Overview of a new operational ice forecasting model," Proceedings of the 9th International Offshore and Polar Engineering Conference (ISOPE '99), Brest, France, Vol. II, pp.622-627.

Sayed, M, and Timco, GW (1999)."A lattice model of ice failure," Proceedings of the 9th International Offshore and Polar Engineering Conference (ISOPE '99), Brest, France, Vol. II, pp.528-534.

Wright, BD (1999)."Evaluation of full scale data for moored vessel stationkeeping in pack ice," Report to the National Research Council on behalf of the Program on Energy Research and Development (PERD) by Brian Wright and Associates, March 1999.

Zhang, J and Hibler, WDIII (1997)."On an efficient numerical method for modelling sea ice dynamics," J. Geophysical Research, Vol. 102, No. C4, pp. 8691-8702.

APPENDIX A: PARTICLE-IN-CELL (PIC) ADVECTION

In the PIC formulation , the ice cover is discretized into individual particles that are advected in a Lagrangian manner. Each particle is considered to have an area and a thickness. For each time step, the particle velocities are determined by interpolating node velocities of an Eulerian grid. Particles can then be advected. The area and mass of each particle are then interpolated back to update the thickness and ice concentration at the Eulerian grid nodes.

A bilinear interpolation function is used to map variables between the particles and the Eulerian grid. For a particle n at location x_p, y_p, and grid node co-ordinates (x_{ij}, y_{ij}), the interpolation coefficients ω would be given by

$$\omega_X(x_{ij}, x_p(n,t)) = [\Delta x - |x_p(n,t) - x_{ij}|]\frac{S_X(i,j,n)}{\Delta x}$$
$$S_X(i,j,n) = \begin{cases} 1 & if \left|x_p(n,t) - x_{ij}\right| \le \Delta x \\ 0 & otherwise \end{cases} \tag{A.1}$$

and

$$\omega_y(x_{ij}, x_p(n,t)) = [\Delta y - |y_p(n,t) - y_{ij}|]\frac{Sy(i,j,n)}{\Delta y}$$
$$S_y(i,j,n) = \begin{cases} 1 & if \left|y_p(n,t) - y_{ij}\right| \le \Delta y \\ 0 & otherwise \end{cases} \tag{A.2}$$

where t is time, and Δx and Δy are the grid cell dimensions.

Thus, the particle velocity components, u_p and v_p can be calculated as follows

$$u_p(X(n,t)) = \sum_i \sum_j \omega_X(x_{ij}, x_p(n,t))\omega_y(y_{ij}, y_p(n,t))u(i,j),$$
$$v_p(X(n,t)) = \sum_i \sum_j \omega_X(x_{ij}, x_p(n,t))\omega_y(y_{ij}, y_p(n,t))v(i,j) \tag{A.3}$$

where u(i,j) and v(i,j) are the velocity components of the Eulerian velocity grid.

Once particles' velocities are determined, advection of a particle, n at location **X**, can be expressed as

$$\mathbf{X}(n, t+\Delta t) = \mathbf{X}(n,t) + \int_t^{t+\Delta t} \mathbf{u}(\mathbf{X}(n,t'), t')dt' \tag{A.4}$$

where **u** is the particle's velocity vector and Δt is the time step. The integral in Eq. (A.4) can be approximated by

$$\int_t^{t+\Delta t} \mathbf{u}(\mathbf{X}(n,t'), t')dt' = \mathbf{u}(\mathbf{X}^*(n,t))\Delta t,$$
$$\mathbf{X}^* = \mathbf{X}(n,t) + \mathbf{u}(\mathbf{X}(n,t),t)\frac{\Delta t}{2} \tag{A.5}$$

The updated thickness and concentration are determined at each time step by mapping particles' areas and volumes back to the Eulerian grid. In the present case, a staggered B-grid is used. Therefore, the thickness and concentration values correspond to a set of nodes different from those used for the velocities. The values of node concentration $c(x_{ij}, t)$ are determined as follows

$$c(x_{ij}, t) = \sum_n \omega_X(x_{ij}, \mathbf{X}(n,t))\omega_y(x_{ij}, \mathbf{X}(n,t))A(n,t)\frac{1}{\Delta x \Delta y} \tag{A.6}$$

where A(n,t) is the area of particle n. The values of node thickness are then calculated as follows

$$h(x_{ij}, t) = \sum_n \omega_X(x_{ij}, \mathbf{X}(n,t))\omega_y(x_{ij}, \mathbf{X}(n,t))V(n,t)\frac{1}{c(x_{ij}, t)\Delta x \Delta y} \tag{A.7}$$

where V(n,t) is the volume of particle n.

The resulting concentration and thickness are further modified to account for ridging, which may occur if the ice cover converges. If the concentration at a node, according to Eq. (A.6), is larger than unity, its value is adjusted to one. The thickness at that node is also increased to conserve the volume of ice. Such a correction of concentration and thickness is mapped back to the particles.

APPENDIX B: NUMERICAL SOLUTION OF THE MOMENTUM EQUATIONS

A brief overview of the numerical approach is presented here (for details see Zhang and Hibler, 1997). The basic idea is to uncouple the x and y components of the momentum equations, and to linearize the terms involving water drag and ice stress by using velocity values from the previous time step. Furthermore, an iteration loop is added to ensure that plastic yield conditions are satisfied. In the present implementation, we include advection terms (which were not considered by Zhang and Hibler, 1997) by using velocities from the previous time step.

The method is illustrated by considering the x-component momentum equation. The solution consists of two levels. In the 1st level, a first estimate of the velocity is obtained from

$$mass_{ice}\frac{u_1^{n+1} - u_1^n}{\Delta t} - \partial_x\left[\eta\,\partial_x u_1^{n+1}\right] - \partial_y\left[\eta\,\partial_y u_1^{n+1}\right] + c_w\rho_w\left|U_w - \mathbf{u}^n\right|u_1^{n+1}$$
$$= \tau_{air-x} - \partial_x\left[\eta\,\partial_y v^n\right] + \partial_y\left[\eta\,\partial_y v^n\right] + c_w\rho_w\left|U_w - \mathbf{u}^n\right|U_{wx}$$
$$- \partial_x p - u^n\partial_x u^n - v^n\partial_y u^n \tag{B.1}$$

where the superscripts n and n+1 refer to time steps n and n+1 respectively. Note that u and v are the x and y components of the velocity vector, **u**. The subscript 1 refers to the 1st level, and the viscosity coefficient η is evaluated using $\mathbf{u}^n$. The x- components of air drag stress and water velocity are τ_{air-x} and U_{wx}, respectively.

In the 2nd level of the solution, the x-component velocity u^{n+1} is evaluated using an equation similar to Eq. (B.1), but using updated values of η that are calculated using velocities $\mathbf{u}^c$

$$\mathbf{u}^c = \left(\mathbf{u}_1^{n+1} + \mathbf{u}^n\right)/2 \tag{B.2}$$

The spatial derivatives in Eq. (B.1) are evaluated using central difference formulas (e.g. Hibler, 1979). Thus the left-hand side of Eq. (B.1) would have 3 unknown velocities at time step n+1. Solution of Eq. (B.1) is done using point successive over relaxation. The solution of both the 1st and 2nd levels is repeated in an iteration loop, called pseudo time stepping, while updating the η. That iteration loop ensures that plastic yield condition is satisfied.